Nanoscale

PAPER

View Article Online
View Journal

Cite this: DOI: 10.1039/d5nr01098e

Efficient and sustainable preparation of fine particles by a bubble-assisted freeze-dissolving method†

Qiutong Zhang, [a] Jiaqi Luo, [a] Yingchen Wang, [a] Wenhao Yan,[a] Mingting Yuan,[a] Yimin Jia,[a] Qiushuo Yu,*[a] Xinyue Zhai,[a] Yuan Zou[a] and Huaiyu Yang *[b]

The development of fine particles has enabled innovative solutions across energy, environmental, and biomedical applications, driving the demand for cleaner, more efficient, and environmentally friendly synthesis methods. In this study, we present a freeze-dissolving approach as a sustainable and energy-efficient alternative to conventional freeze-drying for the preparation of $KHCO_3$ and $NH_4H_2PO_4$ fine particles. By dripping aqueous solutions of $KHCO_3$ or $NH_4H_2PO_4$ into liquid nitrogen, ice-templated particles were rapidly formed and these ice particles were subsequently dissolved in ethanol below 273.15 K. As the ice quickly dissolved in ethanol, the fine particles formed within the ice templates were released into the solution and collected for characterization, including size distribution analysis, SEM imaging, and powder XRD. Compared with freeze-drying, the freeze-dissolving method yields significantly smaller particles while reducing energy consumption by 99%. Moreover, the first-time introduction of air bubbles during the freeze-dissolving step further reduces particle size and substantially limits agglomeration. This bubble-assisted freeze-dissolving technique proves more effective than non-bubbled methods across a range of initial solute concentrations and ice particle sizes, highlighting its potential as a scalable and eco-conscious strategy for fine particle production.

Received 15th March 2025,
Accepted 24th July 2025

DOI: 10.1039/d5nr01098e

rsc.li/nanoscale

Introduction

Fine particles typically possess a large specific surface area, which holds great significance in scientific research and industrial applications.[1–3] As the particle size decreases, the surface energy of fine particles correspondingly increases.[4,5] This increase not only intensifies the surface-related catalytic[6,7] and adsorption[3] effects but may also alter the electronic structure of the material and the intermolecular interactions.[8–10] Fine particles can be employed in catalytic processes as they offer an extensive surface area to facilitate chemical reactions.[11–13] Furthermore, their high adsorption capability makes them highly valuable in fields such as environmental purification and sensor development. For instance, a study reported the adsorption behavior of superfine powdered activated carbon (SPAC) on typical precursors of nitrosodimethylamine (NDMA), underscoring how reducing particle size significantly enhances adsorption efficiency.[14] Research also investigated the adsorption site accessibility of SPAC incorporated into electrospun polystyrene fibers, revealing that integrating SPAC into fibers is an effective method for applications like water treatment and gas adsorption.[15] An embedded nano-spin sensor was developed for *in situ* detection of gas adsorption within porous organic frameworks.[16] Micro- and nanoscale metal particles may exhibit unique optical or magnetic properties, which could be potentially applied in medical imaging and data storage technologies.[17,18] Moreover, the small size effect and quantum size effect can lead to the physical properties of fine particles, such as electrical properties,[19] thermal properties,[20] and melting point,[21] differing markedly from those of macroscopic materials. This opens new research directions in materials science. These unique properties of fine particles make them play a crucial role in research related to chemical production. Precisely controlling the size,

[a]*School of Chemical Engineering, Northwest University; Chemical Engineering Research Center of the Ministry of Education for Advanced Use Technology of Shanbei Energy; International Science & Technology Cooperation Base of MOST for Clean Utilization of Hydrocarbon Resources, Xi'an, Shaanxi 710069, China. E-mail: yuqiushuo@nwu.edu.cn*
[b]*Department of Chemical Engineering, Loughborough University, Loughborough LE11 3TU, UK. E-mail: H.yang3@lboro.ac.uk*

† Electronic supplementary information (ESI) available. See DOI: https://doi.org/10.1039/d5nr01098e

shape and composition of particles enables researchers to design a new generation of functional materials to address current and future technological challenges and meet the demands of increasingly demanding applications.

In agriculture, the high specific surface area and dispersibility of fine particles enhance fertilizer efficiency. Fine particles of $NH_4H_2PO_4$ have been applied and investigated for their fertilizer effect.[22] The smaller $NH_4H_2PO_4$ particles significantly enhance fertilizer efficiency. Fine particles have a higher specific surface area, increasing contact probability with plant roots. This accelerates nutrient release, ensures more uniform distribution, and allows plants to absorb key nutrients like nitrogen and phosphorus more efficiently. In the food industry and animal husbandry, the good dispersibility and flowability of fine particles improve production efficiency and product quality. In fire-extinguishing applications, small $KHCO_3$ particles from B-FDas show higher efficiency. They quickly cover fire sources and efficiently release fire-extinguishing gases. The smaller $KHCO_3$ particles increase decomposition rates and fire-extinguishing efficiency.[23]

The freeze-dissolving in antisolvent (FDas) method[24–26] has been used to produce nano- and micro-particles. The method involved dropwise addition of a solution of $KHCO_3$ into liquid nitrogen to form spherical ice particles. Subsequently, the ice scaffolds were rapidly dissolved in a cryogenically jacketed beaker with magnetic stirring using a dose of antisolvent ethanol corresponding to five to seven times the $KHCO_3$ solution, and the fine particles were recovered by filtration. Many technologies have been utilized to produce fine particles, such as ball milling, chemical precipitation, and sol–gel methods. Ball milling achieves fine particle sizes through mechanical grinding. However, it may introduce impurities and lead to irregular particle shapes.[27–29] Chemical precipitation forms particles *via* chemical reactions in solution. However, it demands strict control of reaction conditions and often results in particles with a broad size distribution.[30–32] The sol–gel method involves transitioning a solution into a gel to create particles, but it is rather complex and time-consuming.[33–35] The FDas method had a quicker dissolving rate, a smaller equipment footprint, and produced fine particles with better dispersion than conventional freeze-drying (FDry). However, under many conditions, it is still challenging to produce particles below 10 μm and aggregation between particles still needs to be improved.

In this work, we developed a novel method, bubble-assisted freeze-dissolving in antisolvent (B-FDas), which involves the introduction of continuous air bubbles during the freeze-dissolving process. This advanced technique produced smaller fine particles with less agglomeration in both the $KHCO_3$ and $NH_4H_2PO_4$ systems. The study encompassed various initial concentrations ranging from 0.02 g g^{-1} to 0.10 g g^{-1} and frozen ice particle volumes varying from 0.01 to 0.08 cm^3. The resulting products were characterized using powder XRD and SEM. The size distributions were determined. Furthermore, the mechanisms and effects of air bubbles during the freeze-dissolving process were discussed.

Experimental section

Materials

Potassium bicarbonate ($KHCO_3$) was purchased from Tianjin Baishi Chemical Co., Ltd (purity > 99.5%). Ethanol was purchased from Tianjin Damao Chemical Reagent Factory (purity > 99.7%). Liquid nitrogen with purity > 99.8% was purchased from Xi'an Aier Industrial Gas Co., Ltd (China). Ammonium dihydrogen phosphate ($NH_4H_2PO_4$) was purchased from Tianjin Damao Chemical Reagent Factory (purity > 99%). All chemicals were used without further purification. In the whole measurement process, distilled deionized water (conductivity less than 0.5 μS cm^{-1}) produced in our laboratory was used.

Formation of frozen spherical particles

Aqueous solutions of $KHCO_3$ were prepared by dissolving 0.2 g, 0.5 g and 1.0 g of $KHCO_3$ in 10 g of water at 295.15 K. $KHCO_3$ frozen spherical particles with an average volume of 0.04 cm^3 were produced by adding these solutions dropwise into a holding vessel containing approximately 10 mL of liquid nitrogen using a pipette. An aqueous $KHCO_3$ solution with a concentration of 0.02 g g^{-1} was prepared and added it dropwise into liquid nitrogen using different sized pipettes to produce $KHCO_3$ frozen spherical particles with average volumes of 0.06 cm^3 and 0.08 cm^3, respectively. Following the same procedure, aqueous solutions of $NH_4H_2PO_4$ were prepared by dissolving $NH_4H_2PO_4$ in 10 g of water at the same room temperature at concentrations of 0.02 g g^{-1}, 0.06 g g^{-1} and 0.10 g g^{-1}, respectively. Frozen spherical $NH_4H_2PO_4$ particles were produced with an average volume of about 0.04 cm^3. With 0.02 g g^{-1} $NH_4H_2PO_4$, 0.01 cm^3 and 0.04 cm^3 frozen ice spherical particles were obtained.

Production of fine particles

B-FDas (bubble-assisted freeze-dissolving in antisolvent), FDas (freeze-dissolving in antisolvent) and FDry (freeze-drying) were applied to obtain particles of $KHCO_3$ and $NH_4H_2PO_4$, as shown in Fig. 1. The frozen spherical ice particles of $KHCO_3$ or $NH_4H_2PO_4$ were added to the antisolvent ethanol (mass ratio of

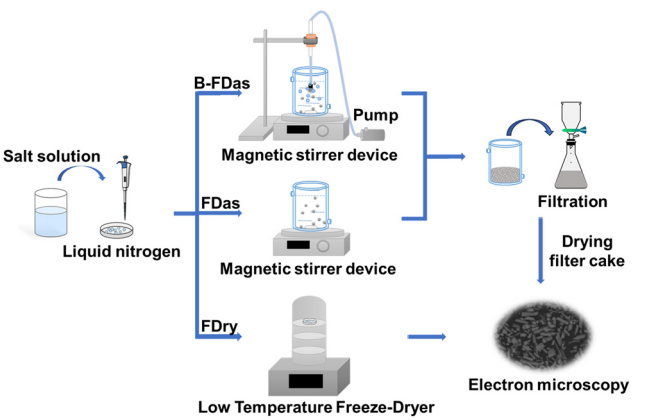

Fig. 1 Schematic diagram of the experimental setup and experimental procedure for B-FDas, FDas and FDry.

inorganic aqueous solution to ethanol: 1 : 7) in a jacketed beaker with continuous stirring at 400 rpm. The jacketed beaker was placed in a cold-water bath at 253.15 K. For the B-FDas method, air bubbles with a diameter of about 900 μm were injected into the solution at a flow rate of 1 L min^{-1}. The temperature of air bubbles was room temperature and approximately 295.15 K. After the ice framework was completely dissolved, the particles were collected after filtration. The different sizes of the frozen spherical particles were used following the same procedure. For the FDry method, the frozen particles were placed in a freeze dryer (FD-1A-50, Beijing Biocon Scientific Instrument Co., Ltd) under freeze temperature and vacuumed conditions until all water molecules sublimated and the particles of $KHCO_3$ and $NH_4H_2PO_4$ were collected.

Dissolving air bubbles

Frozen spherical particles of $KHCO_3$ at a concentration of 0.08 g g^{-1} and a volume of 0.04 cm^3 were used to produce small particles by FDry, and then the product particles were divided into three groups. One group was kept sealed as the original sample and the other two groups were immersed in a mixture of water and ethanol and subjected to stirring with air bubbles and without. The mass ratio of the sample fine particles, water, and ethanol was 0.08 : 1 : 7. The mixing time was always controlled to be 30 seconds and the mixing speed to be 400 rpm for both groups to maintain consistency. After this, the products were collected after filtration.

Characterization

About 0.5 g of product particles were added to 20 mL of ethanol with ultrasonic treatment for 10 minutes. The size distributions of the samples were determined using a Mastersizer 2000 (Malvern). The measurement of each sample was repeated three times and the data provided in the text below represent the equivalent spherical diameter.

The dried product pellets were fixedly placed on the sample stage of the SEM and properly mounted. A scanning electron microscope (TM3000, Hitachi High Technologies Co., Ltd, Japan) was activated to calibrate the relevant parameters to ensure the clarity and accuracy of the images, and the quality and level of detail of the images were controlled by adjusting the scanning speed and scanning range of the electron microscope. The acquired images were processed and analyzed to obtain clearer and more accurate images.

The product samples were ground, pressed and coated to obtain a flat and homogeneous sample surface. The samples prepared were placed in the sample holder of the XRD instrument and a SmartLab powder diffractometer with radiation (1.5406 Å) was used to determine the powder X-ray diffraction of the product samples.

The crystallinity (X_C) of the product samples was evaluated by analysing the XRD patterns using Origin software following eqn (1).

$$X_C = \frac{A_C}{A_C + A_a} \quad (1)$$

where A_C represents the area of crystalline diffraction peaks in the XRD pattern and A_a represents the area of amorphous (or non-crystalline) scattering in the XRD pattern.

Results and discussion

Influences of different sizes of frozen spherical particles

As illustrated in Fig. 2, a comparison of the particle size distributions for fine particles prepared using three different

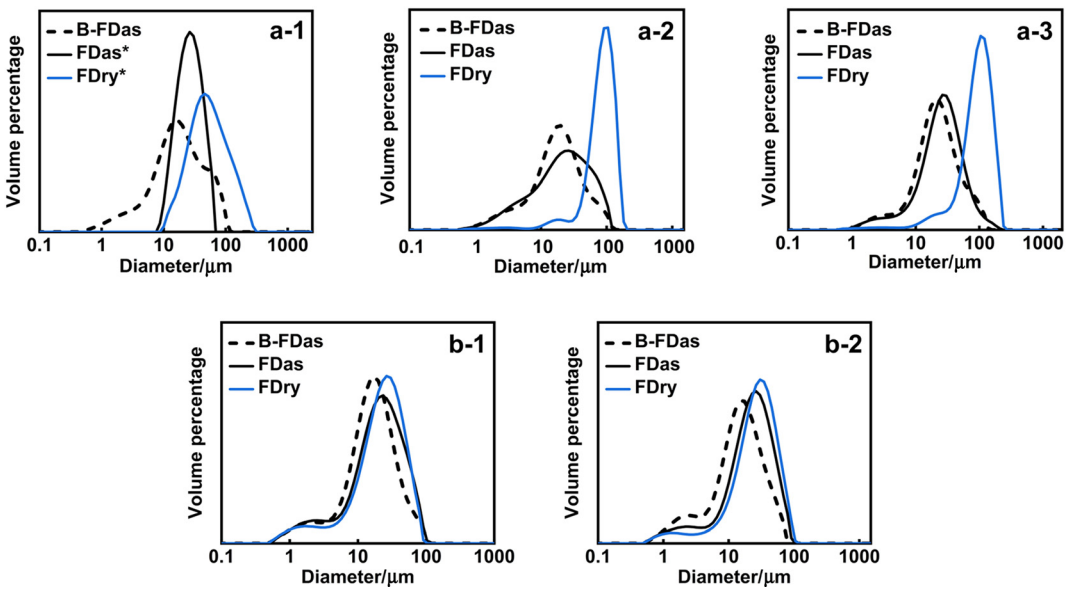

Fig. 2 In the three methods (B-FDas, FDas[25] and FDry[25]), at a concentration of 0.02 g g^{-1}, the particle size distribution of $KHCO_3$-frozen spherical particles has three different average volumes: (a-1) 0.04 cm^3, (a-2) 0.06 cm^3 and (a-3) 0.08 cm^3; the particle size distribution of $NH_4H_2PO_4$-frozen spherical particles has different average volumes: (b-1) 0.01 cm^3 and (b-2) 0.04 cm^3.

methods reveals that the B-FDas method produces significantly smaller particle size distributions compared to the FDas and FDry methods across all three frozen spherical particle sizes. This trend is consistent for both the $KHCO_3$ and $NH_4H_2PO_4$ systems. The results indicate that the introduction of gas bubbles effectively contributes to reducing particle size.

Table 1 shows the $KHCO_3$ particles obtained by the B-FDas method, which consistently produces significantly smaller average particle sizes across all three frozen spherical particle volumes. With frozen particles of 0.04 cm^3, the average size of the final products is 10.20 ± 0.63 μm with B-FDas, compared to 24.70 ± 0.55 μm with FDas and 101.40 ± 0.84 μm with FDry. When the frozen particle size is increased to 0.08 cm^3, B-FDas leads to smaller particle sizes (13.11 ± 0.89 μm) compared with particles obtained with FDas (15.85 ± 0.99 μm) and particles obtained with FDry (103.61 ± 2.41 μm). A similar trend is observed with $NH_4H_2PO_4$ particles, where B-FDas consistently leads to smaller sizes; for examplewhen the frozen particle size is increased to 0.04 cm^3, the average size of the products is 13.67 ± 0.73 μm with B-FDas compared to 20.87 ± 0.94 μm with FDas and 25.25 ± 1.07 μm with FDry.

Table 1 shows that despite the increase in the volume of $KHCO_3$ frozen ice particle sizes from 0.04 cm^3 to 0.08 cm^3, the average size of fine particles prepared by the B-FDas method remains stable at approximately 10 μm. Nevertheless, it is notable that the average sizes of fine particles obtained with both the FDas and FDry methods are larger than that obtained with the B-FDas method. In the $KHCO_3$ system, the average particle sizes of the small particles obtained by the FDry method are all approximately 100 μm, which is significantly larger than the particles obtained with the B-FDas method. The fine particles of $KHCO_3$ and $NH_4H_2PO_4$ obtained by the B-FDas method have a uniform particle size distribution, proved by relatively small span values under all the conditions. For $KHCO_3$, fine particles with frozen particle volumes of 0.04 cm^3, 0.06 cm^3, and 0.08 cm^3 have span values of 2.03, 1.98, and 1.90, respectively. For $NH_4H_2PO_4$, fine particles with frozen particle volumes of 0.01 cm^3 and 0.04 cm^3 have span values of 1.84 and 1.95, respectively. The fine particles obtained by the FDas and FDry methods have similar span values to those obtained by B-FDas, because the average size of D50 is larger. Compared with the values of D90–D10, the fine particles obtained by B-FDas are smaller than those obtained by the FDas and FDry methods.

Fig. 3 and 4 show the SEM images of $KHCO_3$ and $NH_4H_2PO_4$ fine particles. Particles obtained with B-FDas have less agglomeration. It is noted that the morphology of $KHCO_3$ particles obtained by FDas and FDry in this work is consistent with those in previous reports.[25] Fig. 3 shows that $KHCO_3$ particles obtained by the B-FDas method are much smaller particles compared to those obtained with the other two techniques. The particles produced by B-FDas have a regular morphology with minimal aggregation. In contrast, particles prepared by the FDas and FDry methods exhibit significant aggregation. $KHCO_3$ particles obtained by the FDry method show irregularly shapes with extensive aggregation. Fig. 4 shows that $NH_4H_2PO_4$ particles obtained by the B-FDas method have a more consistent and regular morphology, while those obtained by the FDas and FDry methods result in larger and heavily aggregated particles.

The XRD patterns in Fig. 5 show that the $KHCO_3$ and $NH_4H_2PO_4$ fine particles obtained with all three methods, B-FDas, FDas and FDry, as well as raw materials, had good crystalline structures. We can observe that although three different methods were used to obtain fine particles, their XRD images showed a high degree of consistency. The diffraction peaks of each group of samples can correspond to each other, which shows that the obtained $KHCO_3$ and $NH_4H_2PO_4$ fine particles maintained the same phase in the crystal structure regardless of whether they are obtained by the B-FDas, FDas or FDry method. The crystallinity values of the samples based on eqn (1) for the $KHCO_3$ products obtained by the B-FDas, FDas, and FDry methods and that of the raw material were 0.78, 0.77, 0.78, and 0.79, respectively. The crystallinity values of $NH_4H_2PO_4$ products obtained by the B-FDas, FDas, and FDry methods and that of the raw material were 0.82, 0.81, 0.83, and 0.85, respectively. All products, as well as raw materials, had high crystallinity. These results not only confirm the reliability of the preparation method, but also demonstrate that the introduction of gas bubbles did not alter the crystal structure of the material.

Table 1 Average particle size of fine particles obtained by B-FDas, FDas and FDry for different sizes of frozen spherical particles

Frozen ice particle size	0.04 cm^3	0.06 cm^3	0.08 cm^3
$KHCO_3$	Average particle size ± standard deviation (span/μm)		
B-FDas	10.20 ± 0.63 (2.03)	10.96 ± 0.79 (1.98)	13.11 ± 0.89 (1.90)
FDas	24.70 ± 0.55 (1.44)[a]	13.25 ± 0.85 (2.17)	15.85 ± 0.99 (1.69)
FDry	101.40 ± 0.84 (2.79)[a]	93.94 ± 2.56 (1.36)	103.61 ± 2.41 (1.61)

Frozen ice particle size	0.01 cm^3	0.04 cm^3
$NH_4H_2PO_4$	Average particle size ± standard deviation (span/μm)	
B-FDas	14.94 ± 0.77 (1.84)	13.67 ± 0.73 (1.95)
FDas	19.00 ± 0.87 (1.98)	20.87 ± 0.94 (1.80)
FDry	21.23 ± 0.95 (1.87)	25.25 ± 1.07 (1.88)

[a] $KHCO_3$ was obtained using both FDas and FDry methods.[25] For both $KHCO_3$ and $NH_4H_2PO_4$, the concentration at various volumes was maintained at 0.02 g g^{-1}. Span = (D90 − D10)/D50.

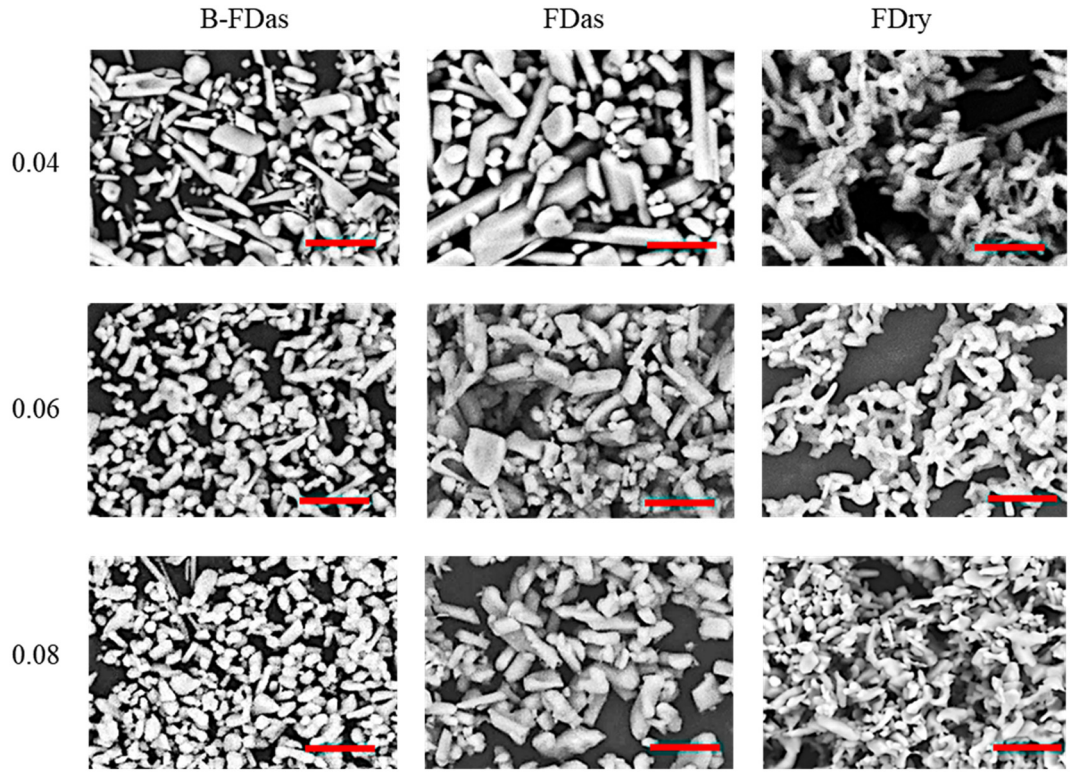

Fig. 3 SEM images of $KHCO_3$ crystalline particles obtained by the B-FDas (left), FDas (middle) and FDry (right) methods from the frozen spherical particles with average sizes of 0.04 cm^3 (top), 0.06 cm^3 (middle) and 0.08 cm^3 (bottom). Scale bar: 10 μm.

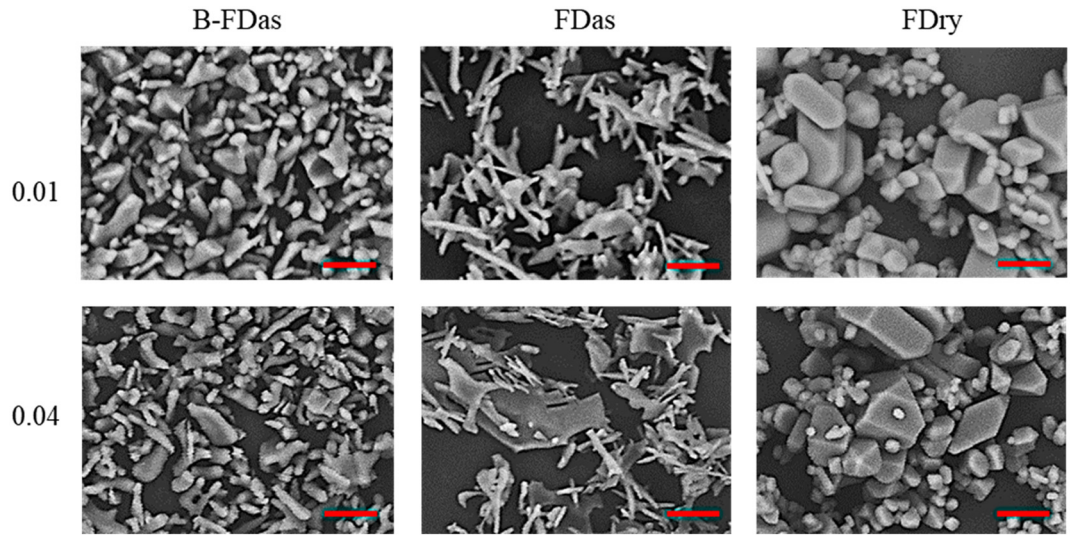

Fig. 4 SEM images of $NH_4H_2PO_4$ crystalline particles obtained by the B-FDas (left), FDas (middle) and FDry (right) methods from the frozen spherical particles with average sizes of 0.01 cm^3 (top) and 0.04 cm^3 (bottom). Scale bar: 10 μm.

Influences of different concentrations of the solution

Fig. 6 shows that the products obtained with the B-FDas method are smaller under all conditions. The particle size increases as the concentration of solution increases. The particles obtained with FDas and FDry are larger, especially at higher concentrations of solution for preparing the frozen particles.

Table 2 shows that the particles obtained by B-FDas have the smallest average particle sizes for both $KHCO_3$ and $NH_4H_2PO_4$ systems, ranging from 10.20 ± 0.63 μm to 13.64 ± 0.72 μm for $KHCO_3$, compared to those with much larger sizes

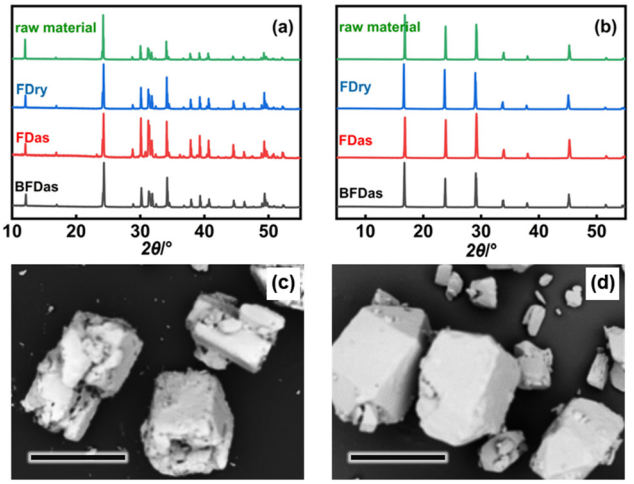

Fig. 5 Powder X-ray diffraction patterns (a) $KHCO_3$ and (b) $NH_4H_2PO_4$ for the raw material and the product particles obtained by the B-FDas, FDas, and FDry methods. The product particles were obtained from frozen ice particles with a volume of 0.04 cm^3 in 0.02 g g^{-1} solution. SEM images of the raw materials of (c) $KHCO_3$ and (d) $NH_4H_2PO_4$. Scale bar: 1 mm.

obtained with FDas and FDry, which can reach up to 148.40 ± 1.02 μm. As the concentration of $NH_4H_2PO_4$ solution increases, the particles produced by the B-FDas method become smaller and more uniform, with the particle size increasing from 13.67 ± 0.73 μm with a solution of 0.02 g g^{-1} concentration to 18.10 ± 0.87 μm with a solution of 0.10 g g^{-1} concentration. The particles produced by the FDas method show an increase in particle size as the concentration increased, increasing from 20.87 ± 0.94 μm at a concentration of 0.02 g g^{-1} to 24.31 ± 0.95 μm at a concentration of 0.10 g g^{-1}. Furthermore, the particles produced by the FDry method are larger, with a maximum size of 68.27 ± 1.62 μm. The particles produced by the B-FDas method had a higher proportion of smaller particles.

Under various concentration conditions, the span values of the products obtained by the B-FDas method remain similar. In the $KHCO_3$ system, when the solution concentration increased from 0.02 g g^{-1} to 0.10 g g^{-1}, the span values of the fine products obtained by the B-FDas method are in the range of 2.03–2.24. The span values of the fine products obtained by the FDas and FDry methods are in the ranges of 1.44–1.89 and 2.11–2.79, respectively. In the $NH_4H_2PO_4$ system, the span values of all fine products are in the range of 1.7–2.0 and the average size of the fine products obtained by the B-FDas method is the smallest, followed by the products obtained by the FDas and FDry methods.

Fig. 7 and 8 show that the $KHCO_3$ and $NH_4H_2PO_4$ particles prepared by B-FDas have more regular shapes. In contrast, the particles prepared by FDas have more irregular shapes with heavier agglomeration. This may be because the presence of air bubbles reduces the contact between particles, thus reducing the possibility of agglomeration. In contrast, particles obtained with FDry are the largest with the heaviest agglomeration. Less agglomeration of the particles obtained with the B-FDas method could improve flowability.

The SEM images show that the morphologies of the fine particles are different for $KHCO_3$ and $NH_4H_2PO_4$ in a similar

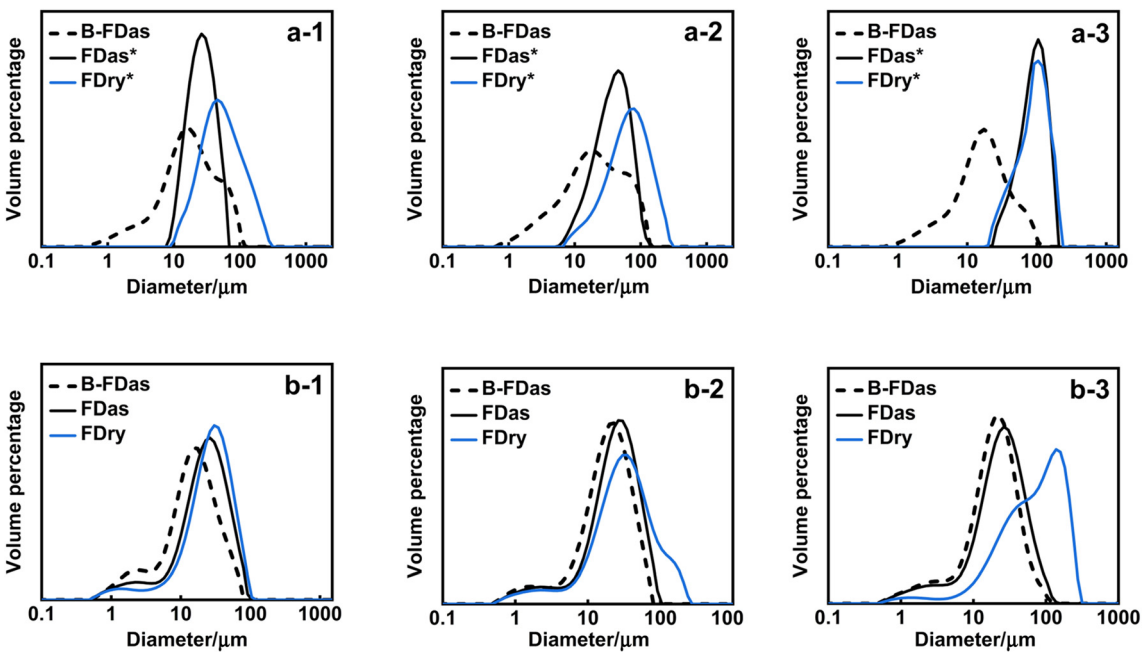

Fig. 6 The particle size distribution of $KHCO_3$ fine particles obtained by the three methods at three concentrations: (a-1) 0.02 (the same as Fig. 2(a-1)), (a-2) 0.05, and (a-3) 0.10 g g^{-1}. The particle size distribution of $NH_4H_2PO_4$ fine particles obtained by the three methods at three concentrations: (b-1) 0.02 (the same as Fig. 2(b-1)), (b-2) 0.06, and (b-3) 0.10 g g^{-1}. The volumes of both types of particles at various concentrations were 0.04 cm^3. *FDas and FDry of $KHCO_3$.[25]

Table 2 Average particle size of fine particles obtained by B-FDas, FDas and FDry for different concentrations of frozen spherical particles

Concentration	0.02 g g^{-1}	0.05 g g^{-1}	0.10 g g^{-1}
$KHCO_3$	Average particle size ± standard deviation (span/μm)		
B-FDas	10.20 ± 0.63 (2.03)	11.21 ± 0.63 (2.19)	13.64 ± 0.72 (2.24)
FDas	24.70 ± 0.55 (1.44)[a]	55.80 ± 0.74 (1.89)[a]	143.59 ± 1.09 (1.77)[a]
FDry	101.40 ± 0.84 (2.79)[a]	148.40 ± 1.02 (2.21)[a]	146.20 ± 1.46 (2.11)[a]
Concentration	0.02 g g^{-1}	0.06 g g^{-1}	0.10 g g^{-1}
$NH_4H_2PO_4$	Average particle size ± standard deviation (span/μm)		
B-FDas	13.67 ± 0.73 (1.95)	17.69 ± 0.88 (1.75)	18.10 ± 0.87 (1.73)
FDas	20.87 ± 0.94 (1.80)	22.60 ± 0.99 (1.74)	24.31 ± 0.95 (1.81)
FDry	25.25 ± 1.07 (1.88)	28.90 ± 1.00 (1.88)	68.27 ± 1.62 (1.93)

[a] FDas and FDry of $KHCO_3$.[25] The volumes of the two particles at various concentrations were both 0.04 cm^3. Span = (D90 − D10)/D50.

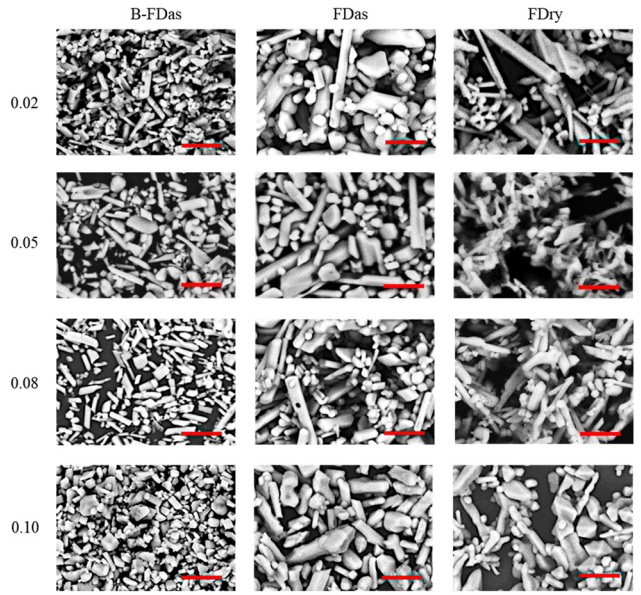

Fig. 7 The SEM images of $KHCO_3$ crystalline microparticles prepared with B-FDas (left), FDas (center), and FDry (right) using frozen spherical particles at concentrations of 0.02 g g^{-1} (first row), 0.05 g g^{-1} (second row), 0.08 g g^{-1} (third row), and 0.10 g g^{-1} (fourth row), respectively. The volume of the prepared frozen spherical particles was 0.04 cm^3. Scale bar: 10 μm.

range of supersaturation with the same freeze dissolving process, which were determined by the properties of materials and compounds. Besides, as the fine particles were formed during the freezing process, the morphology of the particles will be dependent on supersaturation. With higher supersaturation, resulting from a faster freezing rate, smaller droplet volume or higher concentration in the droplet solution, the particles tended to be smaller or to be needle-shaped. The dissolving process would also influence the morphology, but the effect was much more limited than the freezing process. The dissolving process could lead to the dissolution of some of the very tiny particles or breakage of the needle crystals by air bubbles inside the solution.

Function of gas bubbles in freeze dissolving

With air bubbles during the whole dissolving process (0 min–5 min), the $KHCO_3$ particles, as shown in Fig. 9a, are obviously smaller than those obtained without air bubbles, shown in Fig. 9b. The particles obtained with air bubbles during the first half and second half processes are shown in Fig. 9c and d. With air bubbles during the first half of the dissolving process (0 min–2.5 min), the particles are like the products obtained without air bubbles, as shown in Fig. 9a. With air bubbles during the second half of the dissolving process (2.5 min–5 min), the products obtained are like the products obtained with air bubbles during the whole process, as shown in Fig. 9d. The average sizes of these conditions are in the order of particles obtained without air bubbles > particles obtained with air bubbles during 0 min–2. 5 min > particles obtained with air bubbles during 2.5 min–5 min > particles obtained with air bubbles during 0 min–5 min. Therefore, the air bubbles applied in both the first half dissolving process and the second half dissolving process have led to a decrease in the particle size.

During the dissolving process, the presence of air bubbles in the solution led to the formation of smaller particles compared to conditions without bubbles. This size reduction is attributed to the cavitation effects generated by air bubbles, which enhance particle breakage and accelerate the dissolution rate.[36] The fragmentation of tiny ice parts from the larger frozen particles facilitates faster dissolution of both the fragments and the bulk frozen mass. Moreover, the dynamics of air bubbles, such as attachment, detachment, and collapse, could induce shaking, rotation or other movements of the frozen particles.[37,38] These movements would further enhance mass transfer between the frozen particles and the surrounding solvent, contributing to an increased dissolution rate.

Although a similar duration of air bubble presence appears to have a consistent accelerating effect on dissolution, the results shown in Fig. 9 reveal that air bubbles introduced during the later stage of dissolution have a more pronounced impact than those introduced at the initial stage. This suggests an additional mechanism. We propose that beyond promoting ice dissolution, cavitation may also induce fragmentation of the product crystals, particularly in the case of needle-shaped

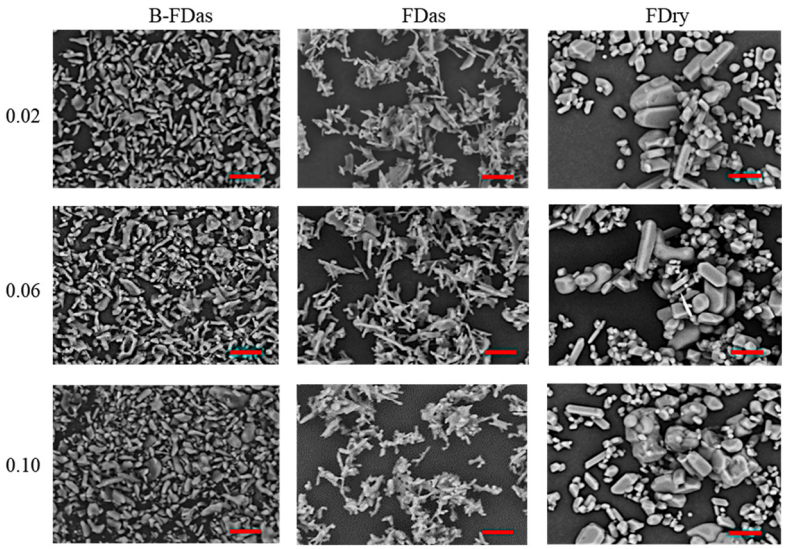

Fig. 8 The SEM images of $NH_4H_2PO_4$ crystalline microparticles prepared with B-FDas (left), FDas (center), and FDry (right) using frozen spherical particles at concentrations of 0.02 g g^{-1} (first row), 0.06 g g^{-1} (second row), and 0.10 g g^{-1} (third row), respectively. The volume of the prepared frozen spherical particles was 0.04 cm^3. Scale bar: 10 μm.

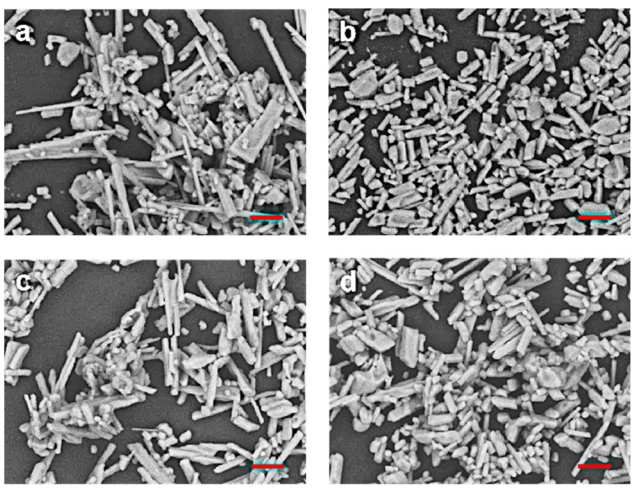

Fig. 9 $KHCO_3$ particles obtained with (a) FDas and (b) B-FDas with air bubbles for 0 min–5 min, (c) with air bubbles only in 0 min–2.5 min and (d) with air bubbles only in 2.5 min–5 min during the dissolving process. The concentration of the $KHCO_3$ solution used was 0.02 g g^{-1} and the average volume of the frozen spherical particles was 0.06 cm^3. Scale bar: 10 μm.

particles. The addition of air bubbles leads to a further decrease in the product crystal size in the later stage when most of the product crystals out of the frozen particles suspended in the solution. In contrast, during the initial stage, the effect was less obvious due to the limited number of product crystals released from the frozen particles in the solution (Fig. 10).

Yield and energy consumption

The yield of the B-FDas method is very high. For example, a 0.10 g g^{-1} $NH_4H_2PO_4$ solution was prepared and 10 g of the solution was frozen in liquid nitrogen to form frozen ice particles. When these frozen particles were added to 70 g of ethanol at −20 °C, the ice parts in the frozen particles were dissolved in the ethanol. After dissolving all the ice parts, the solution because a water and ethanol mixture, with a water and ethanol ratio of about 1 : 7. At −20 °C, the solubility of $NH_4H_2PO_4$ in the mixture solution was very low, with a value of 10^{-3} g g^{-1}. With only about 1% of $NH_4H_2PO_4$ dissolved in the process, about 99% of $NH_4H_2PO_4$ remained in the solution, which could be collected after filtration.

Fig. 11 shows the energy consumption, estimated on the lab scale with consideration of relevant factors, including the entire process of liquid nitrogen production, transportation, and storage, as well as small particle preparation and ethanol recycling. Liquid nitrogen production relies on air separation technology; during transportation and storage, about 15% of the total energy is consumed due to heat transfer and evaporation. In this study, the first step for all three methods is the same: forming frozen spherical particles by dripping $KHCO_3$ and $NH_4H_2PO_4$ solutions into liquid nitrogen. At a temperature of 295.15 K, approximately 60 g of liquid nitrogen was required to prepare 10 g of $KHCO_3$ solution. Approximately 30.8 kJ of energy is required to produce ice particles. However, the actual amount of liquid nitrogen needed under ideal conditions can be much less than the amount consumed during the experiment per unit weight of products.

The FDry method involved placing the frozen particles into a freeze-dryer, which required continuous operation of both a vacuum pump and a compressor under low-temperature vacuum conditions for 24 h. This setup resulted in substantial electricity consumption, with the vacuum pump operating at 400 W and the compressor at 100 W for a total duration of 1440 minutes. In contrast, the FDas and B-FDas methods fol-

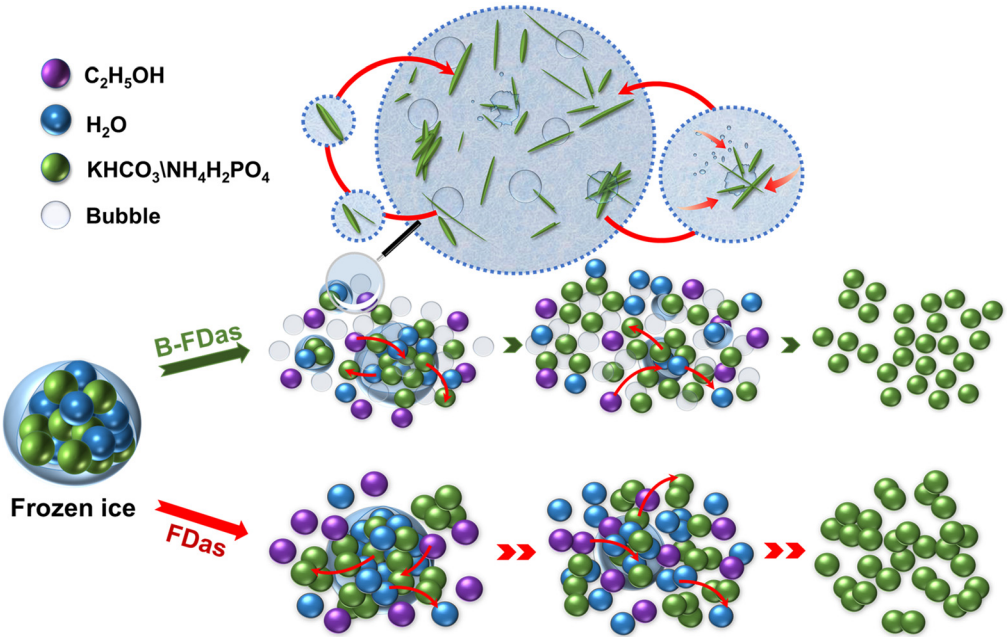

Fig. 10 Proposed mechanisms of freeze dissolving with and without air bubbles.

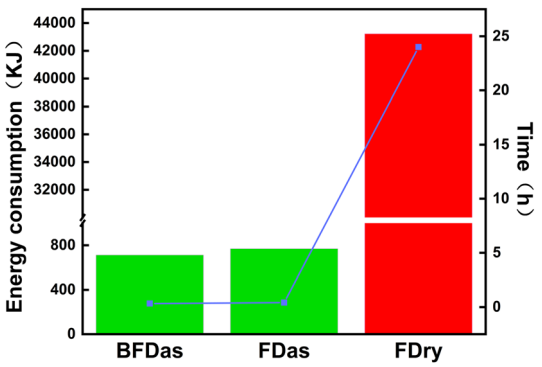

Fig. 11 Comparison of energy and time consumption of the three methods, B-FDas, FDas and FDry. The bar graph depicts energy consumption and the line graph represents the time utilized.

lowed a more energy-efficient three-step process: anti-solvent decomposition, filtration to separate the product, and drying. The FDas method required 15 minutes of operation for a water bath compressor at 200 W, 5 minutes for a filtration pump at 200 W, and 5 minutes for a drying oven at 500 W. The B-FDas method, while incorporating an additional bubble air pump operating at 5 W for 10 minutes, significantly reduced the time required for the anti-solvent decomposition stage, further minimizing energy consumption. The energy consumption of recycling of ethanol and production and transport of liquid nitrogen has been considered.[39–41] Liquid nitrogen can be produced *via* air separation technology, which is essential for all three technologies. The ethanol, used as an anti-solvent for only freeze dissolving technologies, can be recovered through distillation. A comparative calculation of energy consumption (Table S1 in the ESI†) reveals that the total energy consumption for FDry was 43 230.8 kJ, significantly higher than the 769.6 kJ consumed by FDas and the 712.6 kJ required by B-FDas. If the energy consumption for ethanol recovery is excluded, the energy consumption of B-FDas further drops to 363.8 kJ, accounting for less than 1% of that of FDry. These results highlight the energy-intensive nature of the FDry method compared to the more efficient FDas and B-FDas methods. Among them, the B-FDas method proved to be the most energy-efficient, attributed to its shorter processing times and the minimal energy requirements of the bubble generation unit. These findings demonstrate the potential of B-FDas as a remarkably efficient and sustainable approach for fine particle preparation.

The B-FDas method represents a sustainable and efficient approach for producing fine particles. For further scaling up, a large quantity of spherical ice particles will be produced in the first step. Spraying with a suitable nozzle will be required to control the droplet size during injection into liquid nitrogen. It would be valuable to explore the applicability of this technology to other systems, such as in the fields of medicine and catalysis, where the production of particles at the nanometer scale is often required.[42–45] To apply this technology for producing nano-particles of target chemicals, including inorganic and organic compounds,[46,47] two compatible solvents are required. One solvent has high solubility for the target product and it should have a relatively high freezing point. The other one is an anti-solvent with low solubility for the target product and a lower freezing point than the first solvent. The process involves freezing the solution of the target chemicals in the first solvent to form frozen particles. Then the frozen particles are dissolved in the anti-solvent at a controlled temperature

between the freezing points of the first solvent and the anti-solvent. The frozen parts (frozen parts of the first solvent) in the particles can dissolve and the nanosized product remains dispersed in the anti-solvent.

In summary, this study introduces a novel B-FDas method for micro-particle preparation, which demonstrates significant advantages over the conventional FDry method. The B-FDas method not only produces smaller particles and less agglomeration but also exhibits remarkably lower energy consumption and a faster processing speed. Its applicability to both inorganic and organic compounds highlights its potential for widespread use in the preparation of micro- and nano-particles. The insights gained from this research pave the way for more efficient and sustainable particle production technologies. Other technologies for enhancing the mass transfer, such as ultrasound and wet milling, could be further explored.

Conclusions

In this study, we developed an innovative technique with air bubbles during the freeze-dissolving (B-FDas) process to produce fine particles. Compared with the freeze-drying (FDry) method, the particles obtained with B-FDas have a smaller size and lighter agglomeration. The trend is consistent in both $KHCO_3$ and $NH_4H_2PO_4$ systems, with frozen particles from 0.01 to 0.08 cm^3 and solution concentrations from 0.02 g g^{-1} to 0.10 g g^{-1}. Smaller microparticles are obtained with lower solution concentration and smaller frozen particle volume with the B-FDas method. The smallest microparticles of $KHCO_3$ and $NH_4H_2PO_4$ obtained by the B-FDas method are 10.20 ± 0.63 μm and 13.67 ± 0.73 μm, respectively. The particles obtained by FDas are bigger and the particles obtained by FDry are the largest under the same conditions. All the fine particles show good crystalline structures, but the shape of the particles obtained by B-FDas are usually more regular. The energy consumption of B-FDas is less than 1% of the use by FDry, while its processing speed is 100 times faster.

Author contributions

Qiutong Zhang: data curation, visualization, writing – original draft, writing – review & editing, investigation, validation, methodology, and software. Jiaqi Luo: supervision and methodology. Yingchen Wang: methodology. Wenhao Yan: software. Yimin Jia: investigation. Mingting Yuan: formal analysis. Yuan Zou: formal analysis. Xinyue Zhai: investigation. Qiushuo Yu: methodology, project administration, resources, conceptualization, funding acquisition, and supervision. Huaiyu Yang: methodology, conceptualization, writing – review & editing, project administration, and supervision. The manuscript was written through contributions from all authors. All authors have given approval to the final version of the manuscript.

Conflicts of interest

There are no conflicts to declare.

Data availability

The data associated with this article are available on the Mendeley Data platform. The dataset includes two Excel spreadsheets, containing detailed particle size distribution data. These spreadsheets are essential for understanding the results and methodology of this study. The dataset can be accessed *via* the following link: **https://data.mendeley.com/preview/yg3fmrfdb7?a=d2c40398-c3e5-480c-8122-bfeb5ed4b906**.

The data are intended for academic research purposes only and are not to be used for commercial or other non-academic purposes. Users are required to acknowledge the original source and authors when using or referencing the data.

For further information or assistance with data access, please contact the corresponding author at H.yang3@lboro.ac.uk or visit the Mendeley Data support page.

Acknowledgements

The authors are grateful to the National Science Foundation (NSFC21978234) for financial assistance for this project.

References

1 N. Ichinose, Y. Ozaki and S. Kashū, Fundamentals of Superfine Particles, in *Superfine Particle Technology*, Springer London, London, 1992, pp. 1–19. DOI: **10.1007/978-1-4471-1808-4_1**.

2 L. Wang, H. Ji, S. Wang, L. Kong, X. Jiang and G. Yang, Preparation of Fe3O4 with high specific surface area and improved capacitance as a supercapacitor, *Nanoscale*, 2013, **5**, 3793, DOI: **10.1039/c3nr00256j**.

3 O. G. Apul, N. Hoogesteijn von Reitzenstein, J. Schoepf, D. Ladner, K. D. Hristovski and P. Westerhoff, Superfine powdered activated carbon incorporated into electrospun polystyrene fibers preserve adsorption capacity, *Sci. Total Environ.*, 2017, **592**, 458–464, DOI: **10.1016/j.scitotenv.2017.03.126**.

4 D. Vollath, F. D. Fischer and D. Holec, Surface energy of nanoparticles – influence of particle size and structure, *Beilstein J. Nanotechnol.*, 2018, **9**, 2265–2276, DOI: **10.3762/bjnano.9.211**.

5 M. A. Ibrahim, M. Z. Jaafar, M. A. M. Yusof, C. A. Shye and A. K. Idris, Influence of size and surface charge on the adsorption behaviour of silicon dioxide nanoparticles on sand particles, *Colloids Surf., A*, 2023, **674**, 131943, DOI: **10.1016/j.colsurfa.2023.131943**.

6 R. A. Arnold, I. L. Motta and J. M. Hill, Impact of particle size and catalyst dispersion on gasification rates measured in a thermogravimetric analysis unit: Case study of carbon

black catalyzed by potassium or calcium, *Fuel*, 2021, **288**, 119677, DOI: 10.1016/j.fuel.2020.119677.

7 S. Cao, F. (Feng) Tao, Y. Tang, Y. Li and J. Yu, Size- and shape-dependent catalytic performances of oxidation and reduction reactions on nanocatalysts, *Chem. Soc. Rev.*, 2016, **45**, 4747–4765, DOI: 10.1039/C6CS00094K.

8 N. Hoshyar, S. Gray, H. Han and G. Bao, The Effect of Nanoparticle Size on In Vivo Pharmacokinetics and Cellular Interaction, *Nanomedicine*, 2016, **11**, 673–692, DOI: 10.2217/nnm.16.5.

9 B. J. Abdullah, Size effect of band gap in semiconductor nanocrystals and nanostructures from density functional theory within HSE06, *Mater. Sci. Semicond. Process.*, 2022, **137**, 106214, DOI: 10.1016/j.mssp.2021.106214.

10 T. Gomathi, K. Rajeshwari, V. Kanchana, P. N. Sudha and K. Parthasarathy, Impact of nanoparticle shape, size, and properties of the sustainable nanocomposites, in *Sustainable Polymer Composites and Nanocomposites*, Springer International Publishing, 2019, pp. 313–336. DOI: 10.1007/978-3-030-05399-4_11.

11 S. Jeon, W. Jung, H. Bae, S. Ahn, B. Koo, W. Yu, S. Kim, D. Oh, U. Kim, S. A. Barnett, J. Seo, B. Kim and W. Jung, Concurrent Amorphization and Nanocatalyst Formation in Cu–Substituted Perovskite Oxide Surface: Effects on Oxygen Reduction Reaction at Elevated Temperatures, *Adv. Mater.*, 2024, 2404103, DOI: 10.1002/adma.202404103.

12 S. Sun, H. Li and Z. J. Xu, Impact of Surface Area in Evaluation of Catalyst Activity, *Joule*, 2018, **2**, 1024–1027, DOI: 10.1016/j.joule.2018.05.003.

13 S. Shan, J. Li, Y. Maswadeh, C. O'Brien, H. Kareem, D. T. Tran, I. C. Lee, Z.-P. Wu, S. Wang, S. Yan, H. Cronk, D. Mott, L. Yang, J. Luo, V. Petkov and C.-J. Zhong, Surface oxygenation of multicomponent nanoparticles toward active and stable oxidation catalysts, *Nat. Commun.*, 2020, **11**, 4201, DOI: 10.1038/s41467-020-18017-3.

14 Y. Wang, Z. Zhang, Z. Yin, J. Wang, X. Zhang and C. Chen, Adsorption of typical NDMA precursors by superfine powdered activated carbon: Critical role of particle size reduction, *J. Environ. Sci.*, 2025, **147**, 101–113, DOI: 10.1016/j.jes.2023.10.016.

15 B. Sonmez Baghirzade, P. Biswas, S. Moavenzadeh Ghaznavi, B. Frederick, J. F. Reuther and O. G. Apul, Accessibility of adsorption sites for superfine powdered activated carbons incorporated into electrospun polystyrene fibers, *Chem. Eng. J.*, 2023, **461**, 142009, DOI: 10.1016/j.cej.2023.142009.

16 J. Zhang, L. Liu, C. Zheng, W. Li, C. Wang and T. Wang, Embedded nano spin sensor for in situ probing of gas adsorption inside porous organic frameworks, *Nat. Commun.*, 2023, **14**, 4922, DOI: 10.1038/s41467-023-40683-2.

17 T. T. Truong, S. Mondal, V. H. M. Doan, S. Tak, J. Choi, H. Oh, T. D. Nguyen, M. Misra, B. Lee and J. Oh, Precision-engineered metal and metal-oxide nanoparticles for biomedical imaging and healthcare applications, *Adv. Colloid Interface Sci.*, 2024, **332**, 103263, DOI: 10.1016/j.cis.2024.103263.

18 X. Han, K. Xu, O. Taratula and K. Farsad, Applications of nanoparticles in biomedical imaging, *Nanoscale*, 2019, **11**, 799–819, DOI: 10.1039/C8NR07769J.

19 A. Campos, N. Troc, E. Cottancin, M. Pellarin, H.-C. Weissker, J. Lermé, M. Kociak and M. Hillenkamp, Plasmonic quantum size effects in silver nanoparticles are dominated by interfaces and local environments, *Nat. Phys.*, 2019, **15**, 275–280, DOI: 10.1038/s41567-018-0345-z.

20 Y. Volokitin, J. Sinzig, L. J. de Jongh, G. Schmid, M. N. Vargaftik and I. I. Moiseevi, Quantum-size effects in the thermodynamic properties of metallic nanoparticles, *Nature*, 1996, **384**, 621–623, DOI: 10.1038/384621a0.

21 N. Joshi, N. Mathur, T. Mane and D. Sundaram, Size effect on melting temperatures of alumina nanocrystals: Molecular dynamics simulations and thermodynamic modeling, *Comput. Mater. Sci.*, 2018, **145**, 140–153, DOI: 10.1016/j.commatsci.2017.12.064.

22 J. Morton, R. Tillman and A. Morton, Review of research on pasture yield responses to fine particle application of fertiliser in New Zealand, *N. Z. J. Agric. Res.*, 2019, **62**(2), 210–223, DOI: 10.1080/00288233.2018.1474768.

23 F. Xue, Y. Fu, S. Lu, H. Zhang, *et al.*, Insights into the particle diameter and base chosen for dry powder fire extinguishing agents, *Fire Mater.*, 2024, **47**, 774–783, DOI: 10.1002/fam.3117.

24 Q. Yu, Y. Wang, J. Luo and H. Yang, Freeze-Dissolving Method: A Fast Green Technology for Producing Nanoparticles and Ultrafine Powder, *ACS Sustainable Chem. Eng.*, 2022, **10**, 7825–7832, DOI: 10.1021/acssuschemeng.2c02270.

25 J. Luo, Q. Su, Q. Yu, X. Zhai, Y. Zou and H. Yang, Application of efficient and sustainable freeze-dissolving technology in manufacturing of KHCO3 ultrafine particles, *Green Chem. Eng.*, 2024, **5**, 266–272, DOI: 10.1016/j.gce.2023.07.003.

26 J. Luo, Q. Su, Q. Yu, X. Zhai, Y. Zou and H. Yang, Fast and simple preparation of microparticles of $KHCO_3$ by a freeze-dissolving method with single solvent or additional antisolvent, *RSC Sustainability*, 2023, **1**, 1982–1988, DOI: 10.1039/D3SU00234A.

27 N. Kotake, M. Kuboki, S. Kiya and Y. Kanda, Influence of Dry and Wet Grinding Conditions on Fineness and Shape of Particle Size Distribution of Product in a Ball Mill, *Adv. Powder Technol.*, 2011, **22**(1), 86–92, DOI: 10.1016/j.apt.2010.03.015.

28 L. Wei, S. Abd Rahim, M. Abdullah, A. Yin, M. Ghazali, M. Omar, O. Nemeş, A. Sandu, P. Vizureanu and A. Abdellah, Producing Metal Powder from Machining Chips Using Ball Milling Process: A Review, *Materials*, 2023, **16**(13), 4635, DOI: 10.3390/ma16134635.

29 S. A. R. Alavizadeh, M. Shahbaz, M. Kavanlouei and S. S. Kim, The Effect of Mechanical Milling for Enhanced Recycling Ti6Al4 V Powder from Machining Chips, *Sci. Rep.*, 2025, **15**(1), 444, DOI: 10.1038/s41598-024-84913-z.

30 N. Bagheri, F. Nosratinia, F. Zahakifar and T. Yousefi, The Effect of Operational Parameters on the Properties of Thorium Uranium Oxide Produced via Oxalates' Coprecipitation, *Sci. Rep.*, 2025, **15**(1), 18536, DOI: **10.1038/s41598-025-03675-4**.

31 B. V. Farahani, F. H. Rajabi, M. Bahmani, M. Ghelichkhani and S. Sahebdelfar, Influence of Precipitation Conditions on Precursor Particle Size Distribution and Activity of Cu/ZnO Methanol Synthesis Catalyst, *Appl. Catal., A*, 2014, **482**, 237–244, DOI: **10.1016/j.apcata.2014.05.034**.

32 J. A. Nason and D. F. Lawler, Particle Size Distribution Dynamics during Precipitative Softening: Declining Solution Composition, *Water Res.*, 2009, **43**(2), 303–312, DOI: **10.1016/j.watres.2008.10.017**.

33 G. Valverde Aguilar, Introductory Chapter: A Brief Semblance of the Sol-Gel Method in Research, in *Sol-Gel Method - Design and Synthesis of New Materials with Interesting Physical, Chemical and Biological Properties*, IntechOpen, 2019. DOI: **10.5772/intechopen.82487**.

34 D. Navas, S. Fuentes, A. Castro-Alvarez and E. Chavez-Angel, Review on Sol-Gel Synthesis of Perovskite and Oxide Nanomaterials, *Gels*, 2021, **7**(4), 275, DOI: **10.3390/gels7040275**.

35 D. Bokov, A. Jalil, S. Chupradit, W. Suksatan, M. Ansari, I. H. Shewael, G. H. Valiev and E. Kianfar, Nanomaterial by Sol–Gel Method: Synthesis and Application, *Adv. Mater. Sci. Eng.*, 2021, **2021**, 5102014, DOI: **10.1155/2021/5102014**.

36 E. V. Skorb, H. Möhwald and D. V. Andreeva, Effect of Cavitation Bubble Collapse on the Modification of Solids: Crystallization Aspects, *Langmuir*, 2016, **32**, 11072–11085, DOI: **10.1021/acs.langmuir.6b02842**.

37 E. Loth, Quasi-steady shape and drag of deformable bubbles and drops, *Int. J. Multiphase Flow*, 2008, **34**, 523–546, DOI: **10.1016/j.ijmultiphaseflow.2007.08.010**.

38 X. Xu, J. Zhang, F. Liu, X. Wang, W. Wei and Z. Liu, Rising behavior of single bubble in infinite stagnant non-Newtonian liquids, *Int. J. Multiphase Flow*, 2017, **95**, 84–90, DOI: **10.1016/j.ijmultiphaseflow.2017.05.009**.

39 S. F. J. Rizvi, S. Miran, M. Azam, W. Arif, M. Wasif and H. P. Garcia, Numerical Analysis of a Liquid Nitrogen (LN2) Engine for Efficient Energy Conversion, *ACS Omega*, 2021, **6**, 15663–15673, DOI: **10.1021/acsomega.1c00582**.

40 How on-site nitrogen generation reduces your operating costs. Accessed September 4, 2023. Available. at: **https://maziak.co.uk/news-and-media/how-on-site-nitrogen-generation-reduces-your-operating-costs?__cf_chl_rt_tk=7KYLpfjYpi7oZPW8mxGYV201G.TEl8xf9Bm4otgMYWk-1693807407-0-gaNycGzNDWU**.

41 Y. Guo, S. Chen, S. Ma and C. Liu, Optimization of aqueous ethanol distillation based on Aspen simulation, *Chem. Ind. Eng. Prog.*, 2017, **36**(Suppl. 1), 80–86, DOI: **10.16085/j.issn.1000-6613.2016-2438**.

42 H. Tonbul, A. Sahin, E. Tavukcuoglu, G. Esendagli and Y. Capan, Combination drug delivery with actively-targeted PLGA nanoparticles to overcome multidrug resistance in breast cancer, *J. Drug Delivery Sci. Technol.*, 2019, **54**, 101380, DOI: **10.1016/j.jddst.2019.101380**.

43 M. Cheraghi, B. Negahdari, H. Daraee and A. Eatemadi, Heart targeted nanoliposomal/nanoparticles drug delivery: An updated review, *Biomed. Pharmacother.*, 2017, **86**, 316–323, DOI: **10.1016/j.biopha.2016.12.009**.

44 Y. Mahayni, L. Maurer, F. Auer, A. Hutzler, P. Wasserscheid and M. Wolf, Structure sensitivity of the low-temperature dehydrogenation of perhydro dibenzyltoluene on supported platinum nanoparticles, *Catal. Sci. Technol.*, 2024, **14**, 5464–5473, DOI: **10.1039/D4CY00032C**.

45 G. Prieto, H. Tüysüz, N. Duyckaerts, J. Knossalla, G.-H. Wang and F. Schüth, Hollow Nano- and Microstructures as Catalysts, *Chem. Rev.*, 2016, **116**(22), 14056–14119, DOI: **10.1021/acs.chemrev.6b00374**.

46 J. Luo, Y. Wang, Q. Su, Q. Yu, X. Zhai, Y. Zou, Q. Zhang, W. Yan and H. Yang, Rapid and sustainable production of nano and micro medicine crystals via freeze-dissolving technology, *Powder Technol.*, 2024, **443**, 2753–2765, DOI: **10.1016/j.powtec.2024.119913**.

47 C. Guo, Y. Wang, Q. Su, X. Zhai, Y. Zou, Q. Zhang, W. Yan and H. Yang, A Scalable Freeze-Dissolving Approach to Prepare Ultrafine Crystals for Inhalation: Mechanism and Validation, *Cryst. Growth Des.*, 2024, **24**, 2918–2931, DOI: **10.1021/acs.cgd.4c00018**.